UNIVERSITY
OF TRENTO

**DEPARTMENT OF INFORMATION AND COMMUNICATION TECHNOLOGY**

38050 Povo – Trento (Italy), Via Sommarive 14
http://www.dit.unitn.it

# EFFECTIVE EXPLOITATION OF MULTI-VIEW DATA THROUGH THE ITERATIVE MULTI-SCALING METHOD – AN EXPERIMENTAL ASSESSMENT

Massimo Donelli, Davide Franceschini, Gabriele Franceschini, and Andrea Massa

August 2004

Technical Report DIT-04-068

# Effective Exploitation of Multi-View Data through the Iterative Multi-Scaling Method - An Experimental Assessment

Massimo Donelli, Davide Franceschini, Gabriele Franceschini, and Andrea Massa

Department of Information and Communication Technologies

University of Trento -Via Sommarive, 14 - 38050 Trento - ITALY

Tel.: +39 0461 882057; Fax: +39 0461 882093

E-mail: *andrea.massa@ing.unitn.it*,

{*massimo.donelli*, *davide.franceschini*, *gabriele.franceschini*}*@dit.unitn.it*

Web-site: *http://www.eledia.ing.unitn.it*

# Effective Exploitation of Multi-View Data through the Iterative Multi-Scaling Method - An Experimental Assessment

Massimo Donelli, Davide Franceschini, Gabriele Franceschini, and Andrea Massa

**Abstract**

The reconstruction capabilities of a microwave imaging algorithm can be enhanced by exploiting a multi-view measurement set-up. In the past, different researches have proved that collecting scattering data by probing the unknown scenario from different incidence angles, it allows to acquire more information on the scenario under test. This paper is aimed at verifying such an assumption in a real scenario when the Iterative Multi-Scaling Approach (IMSA) is used to fully exploit multi-view data. In fact, unlike synthetic data, in a real environment more measurements introduce larger systematic errors that could affect the physical constraints used in the inversion procedure and, consequently, the reconstruction process. Thus, the analysis is carried out by considering a set of experimental data concerning different scattering configurations involving single and multiple dielectric scatterers.

**Key words**:

Microwave Imaging, Multi-View System, Iterative Multi-Scaling Approach, Experimental Data.

# 1 Introduction

Each microwave imaging system, aimed at detecting, locating and imaging unknown objects located in inaccessible areas (for a general overview and some applications, see [1] - [4] and the references cited therein), is constituted by two main parts. The algorithmic part consists of a processing unit that performs the inversion of the scattered field data by means of a suitable numerical procedure. On the other hand, the electro-mechanical set-up allows the collection of the measures of the electromagnetic field scattered by the scenario under test. Usually, the measurement setup is designed according to the experimental arrangement, which strongly depends on the problem geometry.

Let us consider an ideal situation where there are not limits to the collection of scattered field measures. Even in such a favorable situation, the amount of collectable information from the measurements is limited [5]. In order to enlarge the information content arising from scattered data, multi-view systems [6] (i.e., systems consisting of a rotating setup that probes the investigation area from different angles of illumination) are commonly used. The imaging process benefits by this improvement as theoretically shown in [7] and numerically confirmed in [8] with several synthetic experiments.

But, the same can be said for real experiments? And, it is true whatever the inversion procedure? And, what is the amount of the improvement over single-view systems? The generalization from synthetic to experimental environments is not obvious. In many practical situations, several unavoidable errors and inaccuracies occur. Just to do some examples, the environmental noise corrupts the measures. Such an event adds to the interferences due to the coupling among emitters and receivers and to the positioning errors of the mechanical system. Consequently, a microwave imaging algorithm operates on an unreliable dataset that could introduce false physical constraints and bring the retrieval process towards false solutions.

On the other hand, the increasing of the number of scattering data corresponds to an enlargement of the solution space and of its dimensionality. Therefore, effective and

reliable inversion techniques, able to deal with such a situation, should be used. In such a framework, this paper focuses on the reconstruction capabilities of the IMSA [9], [10] when dealing with real data to assess "if" and "how much" this method is able to fully exploit multi-view data.

The paper is organized as follows. The mathematical formulation of the IMSA will be resumed in Sect. 2 to introduce in Sect. 3 a representative numerical analysis concerning real data scattered by single- and multiple-scatterers configurations. Some conclusions and remarks will be drawn in Sect. 4.

# 2 Mathematical Formulation

Let us consider the two-dimensional scenario depicted in Figure 1. An unknown scatterer, located in an investigation domain $D_I$, interacts with a set of known probing electromagnetic fields, $E^v_{inc}(x,y),\ v = 1, ..., V$. The background is assumed lossless and non-magnetic while the object is described by means of the contrast function $\tau(x,y) = \varepsilon_r(x,\ y) - 1 - j\frac{\sigma(x,y)}{2\pi f \varepsilon_0},\ (x,\ y) \in D_I,\ \varepsilon_r(x,\ y)$ and $\sigma(x,\ y)$ being the dielectric permittivity and the electric conductivity, respectively. The electromagnetic scattered field $E^v_{scatt}\left(x_{m_{(v)}}, y_{m_{(v)}}\right) \triangleq E^v_{tot}\left(x_{m_{(v)}}, y_{m_{(v)}}\right) - E^v_{inc}\left(x_{m_{(v)}}, y_{m_{(v)}}\right)$ ($E^v_{tot}\,(x,\ y)$ being the electric field in the presence of the scatterer) is collected in $m_{(v)} = 1, ..., M_{(v)}$ positions belonging to an observation domain $D_M$ external to $D_I$.

From a mathematical point of view, the interactions among the scatterer and incident electromagnetic fields are described through the Lippmann-Schwinger integral equations [11], discretized according to the Richmond's procedure [12]:

$$\begin{gathered} E^v_{scatt}\left(x_{m_{(v)}},\ y_{m_{(v)}}\right) = \Im^{v,m}_{Data}\left\{\tau\left(x_n,\ y_n\right),\ E^v_{tot}\left(x_n,\ y_n\right);\ n = 1, ..., N;\ v = 1, ..., V\right\} \\ \left(x_{m_{(v)}},\ y_{m_{(v)}}\right) \in D_M \qquad m_{(v)} = 1, ..., M_{(v)};\quad v = 1, ..., V \end{gathered} \tag{1}$$

$$\begin{gathered} E^v_{inc}\left(x_n,\ y_n\right) = \Im^{v,n}_{State}\left\{\tau\left(x_n,\ y_n\right),\ E^v_{tot}\left(x_n,\ y_n\right);\ n = 1, ..., N;\ v = 1, ..., V\right\} \\ \left(x_n,\ y_n\right) \in D_I \qquad n = 1, ..., N;\quad v = 1, ..., V \end{gathered} \tag{2}$$

where $\tau(x,\, y) = \sum_{n=1}^{N} \tau\,(x_n,\, y_n)\, F_n\,(x,\, y)$ and $E^v_{tot}(x,\, y) = \sum_{n=1}^{N} E^v_{tot}\,(x_n,\, y_n)\, F_n\,(x,\, y)$, $F_n\,(x,\, y)$ being the $n$th basis function; $\Im_{ext}$ and $\Im_{int}$ are the external and internal scattering operators [11].

Such a formulation provides a set of non-linear equations characterized by an intrinsic ill-conditioning. Then, the arising algebraic system (1)-(2) is commonly solved by recasting the problem to the minimization of a suitable cost function.

However, to better exploit the information content of scattered data, a multi-scaling strategy [10] is used by defining a multi-resolution expansion of the unknown quantities as follows

$$\begin{array}{c} \tau(x,\, y) = \sum_{r=1}^{R} \sum_{n_{(r)}=1}^{N_{(r)}} \tau\left(x_{n_{(r)}}, y_{n_{(r)}}\right)\, F_{n_{(r)}}\,(x,\, y) \\ \left(x_{n_{(r)}}, y_{n_{(r)}}\right) \in D_I \qquad n_{(r)} = 1, ..., N_{(r)}; \quad r = 1, ..., R = (s+1) \end{array} \tag{3}$$

$$E^v_{tot}\,(x,\, y) = \sum_{r=1}^{R} \sum_{n_{(r)}=1}^{N_{(r)}} E^v_{tot}\left(x_{n_{(r)}},\, y_{n_{(r)}}\right)\, F_{n_{(r)}}\,(x,\, y) \tag{4}$$

where $R$ defines the maximum order of the resolution (being $r$ the resolution index), and by iteratively performing (at each step $s$ of the process) a reconstruction with an increment of the spatial resolution in the Region-of-Interest (RoI) to which the scatterer belongs.

For a detailed description, let us consider the flow-chart shown in Fig. 2. At the "*initialization*" ($s = 0$), the investigation domain is uniformly partitioned in $N_{(R)}$ ($R = 1$) square sub-domains and the problem unknowns are set to the background configuration ($E^{v\,(s)}_{tot}\left(x_{n_{(R)}},\, y_{n_{(R)}}\right)\Big|_{s=0} = E^v_{inc}\left(x_{n_{(R)}},\, y_{n_{(R)}}\right)$ and $\tau^{(s)}\left(x_{n_{(R)}}, y_{n_{(R)}}\right)\Big|_{s=0} = \tau_0,\ n_{(R)} = 1, ..., N_{(R)}$). Moreover, the multi-resolution cost function is defined [13]

$$\Phi\left\{ \tau^{(s)}_{(q)}\left(x_{n_{(r)}}, y_{n_{(r)}}\right),\, E^{v\,(s)}_{tot}\left(x_{n_{(r)}}, y_{n_{(r)}}\right);\ \begin{array}{c} q = 1, .., Q_{(s)}; \qquad r = 1, ..., R = s; \\ n_{(r)} = 1, ..., N_{(r)}; \qquad v = 1, ..., V \end{array} \right\} = \tag{5}$$

$$\left\{\sum_{q=1}^{Q_{(s)}}\sum_{v=1}^{V}\sum_{m_{(v)}=1}^{M_{(v)}}\left|E_{scatt}^{v}\left(x_{m_{(v)}},y_{m_{(v)}}\right)-\sum_{r=1}^{R}\sum_{n_{(r)}=1}^{N_{(r)}}\left\{w^{(q)}\left(x_{n_{(r)}},y_{n_{(r)}}\right)\tau_{(q)}^{(s)}\left(x_{n_{(r)}},y_{n_{(r)}}\right)\right.\right.$$
$$\left.\left.E_{tot}^{v\,(s)}\left(x_{n_{(r)}},y_{n_{(r)}}\right)G_{2d}\left(A_{n_{(r)}},\rho_{n_{(r)}m_{(v)}}\right)\right\}\right|^{2}\Bigg\}+\Bigg\{\sum_{q=1}^{Q_{(s)}}\sum_{v=1}^{V}\sum_{r=1}^{R}\sum_{n_{(r)}=1}^{N_{(r)}}$$
$$\Bigg\{w^{(q)}\left(x_{n_{(r)}},y_{n_{(r)}}\right)\Bigg|E_{inc}^{v}\left(x_{n_{(r)}},y_{n_{(r)}}\right)-\Bigg[E_{tot}^{v\,(s)}\left(x_{n_{(r)}},y_{n_{(r)}}\right)$$
$$+\sum_{u_{(r)}=1}^{N_{(r)}}\left\{\tau_{(q)}^{(s)}\left(x_{u_{(r)}},y_{u_{(r)}}\right)\quad E_{tot}^{v\,(s)}\left(x_{u_{(r)}},y_{u_{(r)}}\right)G_{2d}\left(A_{u_{(r)}},\rho_{u_{(r)}n_{(r)}}\right)\right\}\Bigg]\Bigg|\Bigg\}^{2}\Bigg\}$$

where

$$w^{(q)}(x_{n_{(r)}},y_{n_{(r)}})=\begin{cases}0 & if\quad (x_{n_{(r)}},y_{n_{(r)}})\notin D_{O(s-1)}^{(q)}\\ 1 & if\quad (x_{n_{(r)}},y_{n_{(r)}})\in D_{O(s-1)}^{(q)}\end{cases}$$

$Q$ being the number of scatterers and $D_O^{(q)}$, $q=1,...,Q$ the corresponding RoIs, where the synthetic zoom will be performed; $Q_{(s=0)}=1$.

Successively ($s\leftarrow s+1$), the unknowns are updated

$$\tau^{(s)}\left(x_{n_{(R)}},y_{n_{(R)}}\right)\Big\rfloor_{s=1}=arg\left\{min_{\tau_{(q)}^{(0)}}\left[\Phi^{(0)}\right]\right\} \tag{6}$$

$$E_{tot}^{v\,(s)}\left(x_{n_{(R)}},\,y_{n_{(R)}}\right)\Big\rfloor_{s=1}=arg\left\{min_{E_{tot}^{v\,(s)}}\left[\Phi^{(0)}\right]\right\} \tag{7}$$

where $\Phi^{(0)}=\Phi\left\{\tau_{(q)}^{(0)}\left(x_{n_{(r)}},y_{n_{(r)}}\right),\,E_{tot}^{v\,(0)}\left(x_{n_{(r)}},y_{n_{(r)}}\right)\right\}$, by minimizing (5) with a suitable optimization algorithm [14].

At this point, the multi-resolution capabilities of the IMSA are fully exploited. The information acquired on the scenario under test allows an estimate of the the number $Q_{(s)}$ of scatterers lying in $D_I$ as well as of the geometrical parameters for each of the corresponding RoIs ("*scatterer localization*" phase and "*estimation of the geometrical parameters*" phase - Fig. 2) [13]. The resolution level is enhanced ($R\leftarrow R+1$) in the RoIs and a new representation of the unknowns is given according to (3) and (4). Then, a new minimization of $\Phi^{(s)}$ is performed by taking into account the so-defined (6)-(7) trial configuration ("*initialization of the new step*" phase - Fig. 2).

Iteratively, such a procedure is repeated until a stationary condition [13] for the recon-

struction is reached ($s = S_{opt}$).

# 3 Numerical Analysis

In this Section, a numerical analysis will be carried out in order to assess the reconstruction capabilities of the IMSA in regard to the multi-view measurement setup by considering real scattered data. Towards this end, some examples of the experimental dataset available at the "Institute Fresnel" - Marseille, France" [15] will be processed.

The first test case considers a single dielectric cylinder ($15\,mm$ in radius) located at ($x_{c_{ref}} = 0.0$, $y_{c_{ref}} = -30\,mm$) and characterized by a homogeneous contrast $\tau(x,\, y) = 2.0 \pm 0.3$ estimated with a waveguide method [16]. Concerning the investigation domain, a square domain $L_{DI} = 30\,cm$ in side has been considered and the reconstruction has been performed by fully exploiting the available scattering data ($M_{(v)} = 49$), but using mono-frequency measurements ($f = 4\,GHz$).

The effects of the multi-view setup, in terms of reconstruction errors, will be analyzed by considering the following quantities

$$\rho = \frac{1}{Q}\sum_{q=1}^{Q}\left\{\frac{\sqrt{\left[x^{(q)}_{c_{(S_{opt})}} - x^{(q)}_{c_{ref}}\right]^2 + \left[y^{(q)}_{c_{(S_{opt})}} - y^{(q)}_{c_{ref}}\right]^2}}{\lambda}\right\} \qquad (Localization\ Error) \tag{8}$$

$$\Delta = \frac{1}{Q}\sum_{q=1}^{Q}\left\{\frac{\left|R^{(q)}_{(S_{opt})} - R^{(q)}_{ref}\right|}{R^{(q)}_{ref}}\right\} \qquad (Dimensional\ Error) \tag{9}$$

where the sub-script "*ref*" indicates actual quantities[(1)] .

As a first experiment, the reconstruction has been carried out with a *bare* CG-based approach. The investigation domain has been uniformly partitioned in $N = 23 \times 23$ square sub-domains. Fig. 3 shows the behavior of the error figures versus the number of views $V$ used by the multi-view acquisition system. As can be observed, the localization

(1) Such quantities are equal to the nominal values reported in [15].

error $\rho$ slightly decreases (from $\rho\rfloor_{V=1} = 1.25 \times 10^{-1}$ up to $\rho\rfloor_{V=30} = 7.17 \times 10^{-2}$) in correspondence with an increasing of the illuminations. On the contrary, an increment of $\Delta$ occurs (from $\Delta\rfloor_{V=1} = 2.96 \times 10^{-1}$ up to $\Delta\rfloor_{V=30} = 6.59 \times 10^{-1}$) as pictorially shown in Fig. 4 where the images of the retrieved profiles when $V = 1$, $V = 6$, $V = 12$, and $V = 24$ are given[(2)]. Such a result seems to indicate that the CG-based approach does not fully exploit the advantages of a multi-view system.

Then, in the second experiment, the same problem has been addressed by using the IMSA with the same CG-based optimizer for the cost function minimization (IMSA-CG Approach). According to the amount of information of the scattering data [7] and at the initialization of the multi-scaling process, $D_I$ has been discretized in $N_{(R)} = 10 \times 10$ $(R = 1)$ square cells.

For comparison purposes, Fig. 5 shows the behavior of the error figures for the two methods. Concerning the IMSA-CG Approach, the localization accuracy benefits of the enlargement of the available information content (similarly to the CG Approach) as well as the dimensional error, which turns out to be $\Delta < 2.0 \times 10^{-1}$ whatever $V$. For completeness, Figs. $6(a)$-$6(b)$ diplay the retrieved profiles when $V = 1$, $V = 6$, $V = 12$, and $V = 24$, respectively.

To generalize these indications, the same analysis has been performed for a multiple-scatterers scenario. Towards this aim, the dataset "*twodielTM_ 8f.exp*" [15], concerned with two circular dielectric ($\tau^{(1)} = \tau^{(2)} = 2.0 \pm 0.3$) cylinders of radius $R_{ref}^{(1)} = R_{ref}^{(2)} = 15\,mm$ placed $90\,mm$ from each other and located at the nominal coordinates ($x_{c_{ref}}^{(1)} = 0.0$, $y_{c_{ref}}^{(1)} = 45\,mm$) and ($x_{c_{ref}}^{(2)} = 0.0$, $y_{c_{ref}}^{(2)} = -45\,mm$), has been processed.

The achieved results, in terms of localization [Fig. $7(a)$] as well as shaping accuracy [Fig. $7(b)$], clearly point out an improvement in the reconstruction allowed by the multi-view setup. Whatever the inversion method, $\rho$ and $\Delta$ significantly reduces by assessing an advantage in the inversion when more views are used. More in detail, as far as the

[(2)] Please note that the black pixel in the lower right border is used for reference and the dashed line indicates the region occupied by the actual scatterer.

localization accuracy is concerned, $\rho$ varies between $\rho\rfloor_{V=1} \simeq 6.0 \times 10^{-1}$ and $\rho\rfloor_{V=30} \simeq 1.0 \times 10^{-1}$ and the IMSA-CG Approach outperforms the bare CG procedure. Similar considerations can be drawn also by observing the behavior of $\Delta$. A non-negligible (if compared to the error values of the CG-based method) improvement in the reconstruction is allowed by the multi-scaling approach when $V \in [1, 16]$ ($\frac{\Delta^{(CG)}\rfloor_{V=1}}{\Delta^{(IMSA-CG)}\rfloor_{V=1}} \simeq 2.80$ and $\frac{\Delta^{(CG)}\rfloor_{V=16}}{\Delta^{(IMSA-CG)}\rfloor_{V=16}} \simeq 1.90$).

Finally, Fig. 8 shows the images of the reconstructed profiles when the CG-Approach [Figs. 8($a$)-8($c$)-8($e$)-8($g$)] and the IMSA-CG Approach [Figs. 8($b$)-8($d$)-8($f$)-8($h$)] are used for $V = 1$ [Figs. 8($a$)-8($b$)], $V = 6$ [Figs. 8($c$)-8($d$)], $V = 12$ [Figs. 8($e$)-8($f$)], and $V = 24$ [Figs. 8($g$)-8($h$)] views, respectively. The two cylinders have been effectively reconstructed, but the reconstruction accuracy gets better when the number of views grows. Moreover, as indicated by the values of the error figures, the retrieval achieved with IMSA-CG Approach turns out to be more close to the actual one when the multi-view setup is adopted. However, it can be remarked that the centers of each cylinders are slightly shifted whatever $V > 1$. Even though such a shift is within the experimental margin, it should be pointed out that a similar behavior has been obtained in several tests with various methods (see [15] for a detailed review). This could suggest that an incorrect positioning occurred during the data measurement.

# 4 Conclusions

In this paper, the effect of a multi-view measurement setup on the reconstruction accuracy of the IMSA has been analyzed. The capabilities of the multi-resolution approach to fully exploit the increment of the information content allowed by the multi-view system have been assessed and compared with those of a standard reference method. As a benchmark, some experimental dataset available at the "Institute Fresnel" - Marseille, have been processed and, notwithstanding the large amount of systematic errors that a real measurement setup introduce, the proposed strategy has shown satisfactory performances.

The obtained results indicate that the IMSA benefits by multi-illumination conditions in a real environment, as well, and it is able to usefully exploit the allowed increment of information.

# References


[1] J. Ch. Bolomey, "New concept for microwave sensing," *Adv. Microw. Millim. Wave Detectors*, vol. 2275, 1994.

[2] K. Louis, "Medical imaging: State of the art and future development," *Inverse Problems*, vol. 8, pp. 709-738, 1992.

[3] R. H. Hoole et al., "Inverse problem methodology and finite elements in the identifications of cracks, sources, materials, and their geometry in inaccessible locations," *IEEE Trans. Magn.*, vol. 27, pp. 3433-3443, 1991.

[4] D. J. Daniels, "Surface penetrating radar," *IEE Electron. Comm. Eng. J.*, vol. 8, pp. 165-182, 1996.

[5] O. M. Bucci and G. Franceschetti, "On the Degrees of Freedom of Scattered Fields," *IEEE Trans. on Ant. and Prop.*, vol. 37, pp. 918-926, 1989.

[6] S. Caorsi, G. L. Gragnani, and M. Pastorino, "A multiview microwave imaging system for two- dimensional penetrable objects," I*EEE Trans. Microwave Theory Tech.*, vol. 39, no. 5, pp. 845-851, 1991.

[7] O. M. Bucci and T. Isernia, "Electromagnetic inverse scattering: Retrievable information and measurement strategies," *Radio Sci.,* vol. 32, pp. 2123-2138, 1997

[8] S. Caorsi, G. L. Gragnani, and M. Pastorino, "An approach to microwave imaging using a multiview moment method solution for a two-dimensional infinite cylinder," *IEEE Trans. Microwave Theory Tech.*, vol. 39, no. 6, pp. 1062-1067, 1991.

[9] S. Caorsi, M. Donelli, D. Franceschini, and A. Massa, "An Iterative Multiresolution Approach for Microwave Imaging Applications," *Microwave Opt. Tech. Lett.,* vol. 32, pp. 352-356, 2002.

[10] S. Caorsi, M. Donelli, D. Franceschini, and A. Massa, "A new methodology based on an iterative multi-scaling for microwave imaging," *IEEE Trans. Microwave Theory Tech.*, vol. 51, pp. 1162-1173, 2003.

[11] D. Colton and R. Krees, *Inverse acoustics and electromagnetic scattering theory.* Berlin, Germany: Springer-Verlag, 1992.

[12] J. H. Richmond, "Scattering by a dielectric cylinder of arbitrary cross section shape," *IEEE Trans. Antennas Propagat.*, vol. 13, pp. 334-341, 1965.

[13] S. Caorsi, M. Donelli, and A. Massa, "Location, detection, and imaging of multiple scatterers by means of the iterative multiscaling method", *IEEE Trans. Microwave Theory Tech.*, vol. 52, pp. 1217-1228, 2004.

[14] R. V. Kohn and A. McKenney, "Numerical implementation of a variational method for electrical impedance tomography," *Inverse Problems*, vol. 6, pp. 389-414, 1990.

[15] K. Belkebir and M. Saillard, Special section: "Testing Inversion Algorithms against Experimental Data," *Inverse Problems*, vol. 17, pp. 1565-1702, 2001.

[16] W. B. Weir, "Automatic measurement of complex dielectric constant and permeability at microwave frequencies," *Proc. IEEE*, vol. 62, pp. 33-36, 1974.

# Figure Captions

- **Figure 1.** Problem geometry.
- **Figure 2.** Flow chart of the Iterative Multi-Scaling Method.
- **Figure 3.** Reconstruction of an off-centered homogeneous circular cylinder (Real dataset "Marseille" [15] - "*dielTM_ dec8f.exp*") - *CG Approach*. Error figures versus $V$.
- **Figure 4.** Reconstruction of an off-centered homogeneous circular cylinder (Real dataset "Marseille" [15] - "*dielTM_ dec8f.exp*") - *CG Approach*. Retrieved profiles at the convergence by considering $(a)$ $V = 1$, $(b)$ $V = 6$, $(c)$ $V = 12$, and $(d)$ $V = 24$ views.
- **Figure 5.** Reconstruction of an off-centered homogeneous circular cylinder (Real dataset "Marseille" [15] - "*dielTM_ dec8f.exp*") - Error figures versus $V$ for the *CG Approach* and the *IMSA-CG Approach*.
- **Figure 6.** Reconstruction of an off-centered homogeneous circular cylinder (Real dataset "Marseille" [15] - "*dielTM_ dec8f.exp*") - *IMSA-CG Approach*. Retrieved profiles at the convergence step $s = S_{opt}$ by considering $(a)$ $V = 1$, $(b)$ $V = 6$, $(c)$ $V = 12$, and $(d)$ $V = 24$ views.
- **Figure 7.** Reconstruction of two homogeneous circular cylinders (Real dataset "Marseille" [15] - "*twodielTM_ 8f.exp*") - Error figures versus $V$ for the *CG Approach* and the *IMSA-CG Approach*.
- **Figure 8.** Reconstruction of two homogeneous circular cylinders (Real dataset "Marseille" [15] - "*twodielTM_ 8f.exp*") - Retrieved profiles at the convergence with the $(a)$ *CG Approach* - $V = 1$, $(b)$ *IMSA-CG Approach* - $V = 1$, $(c)$ *CG Approach* - $V = 6$, $(d)$ *IMSA-CG Approach* - $V = 6$, $(e)$ *CG Approach* - $V = 12$, $(f)$ *IMSA-CG*

*Approach* - $V = 12$, $(g)$ *CG Approach* - $V = 24$, and $(h)$ *IMSA-CG Approach* - $V = 24$.

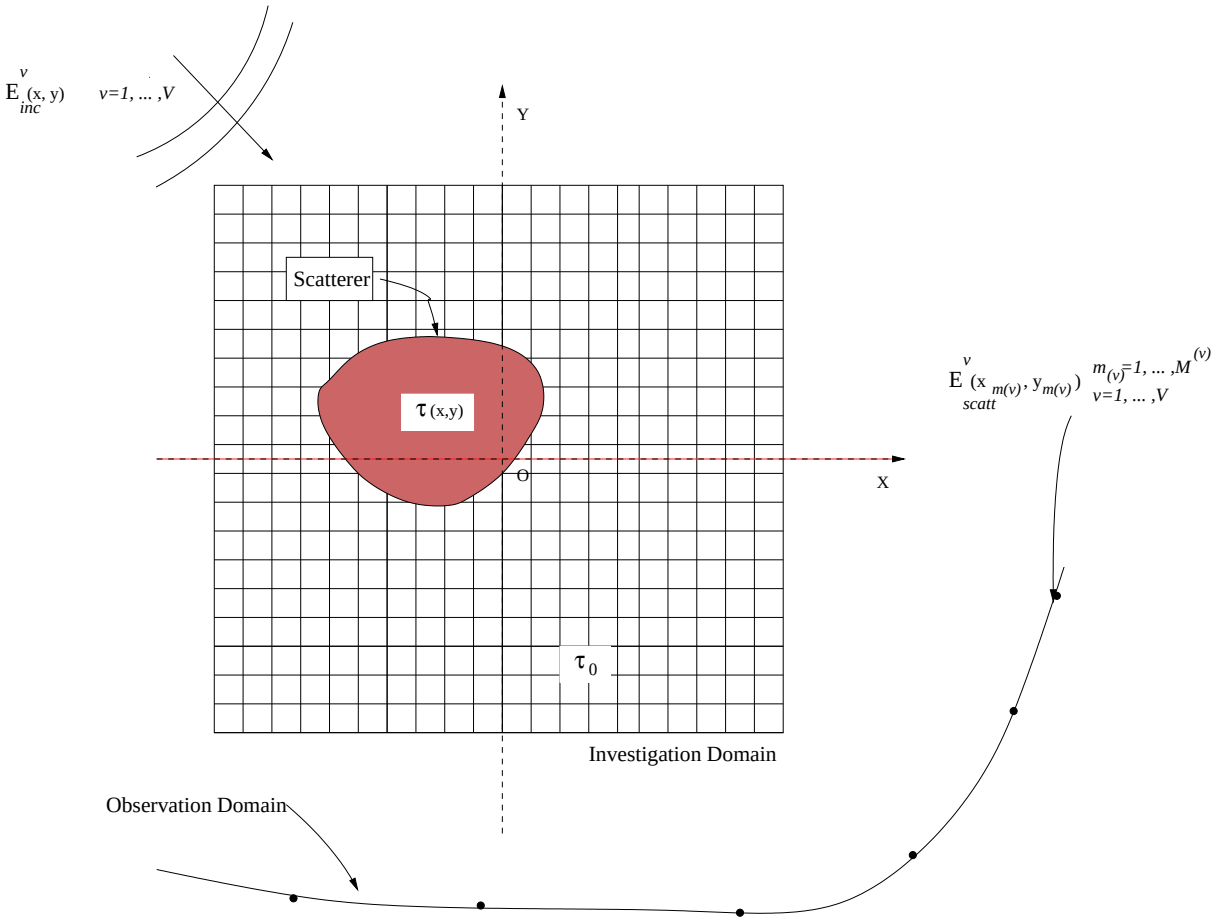


**Figure 1 - M. Donelli *et al.*,** "Effective Exploitation of Multi-View Data..."

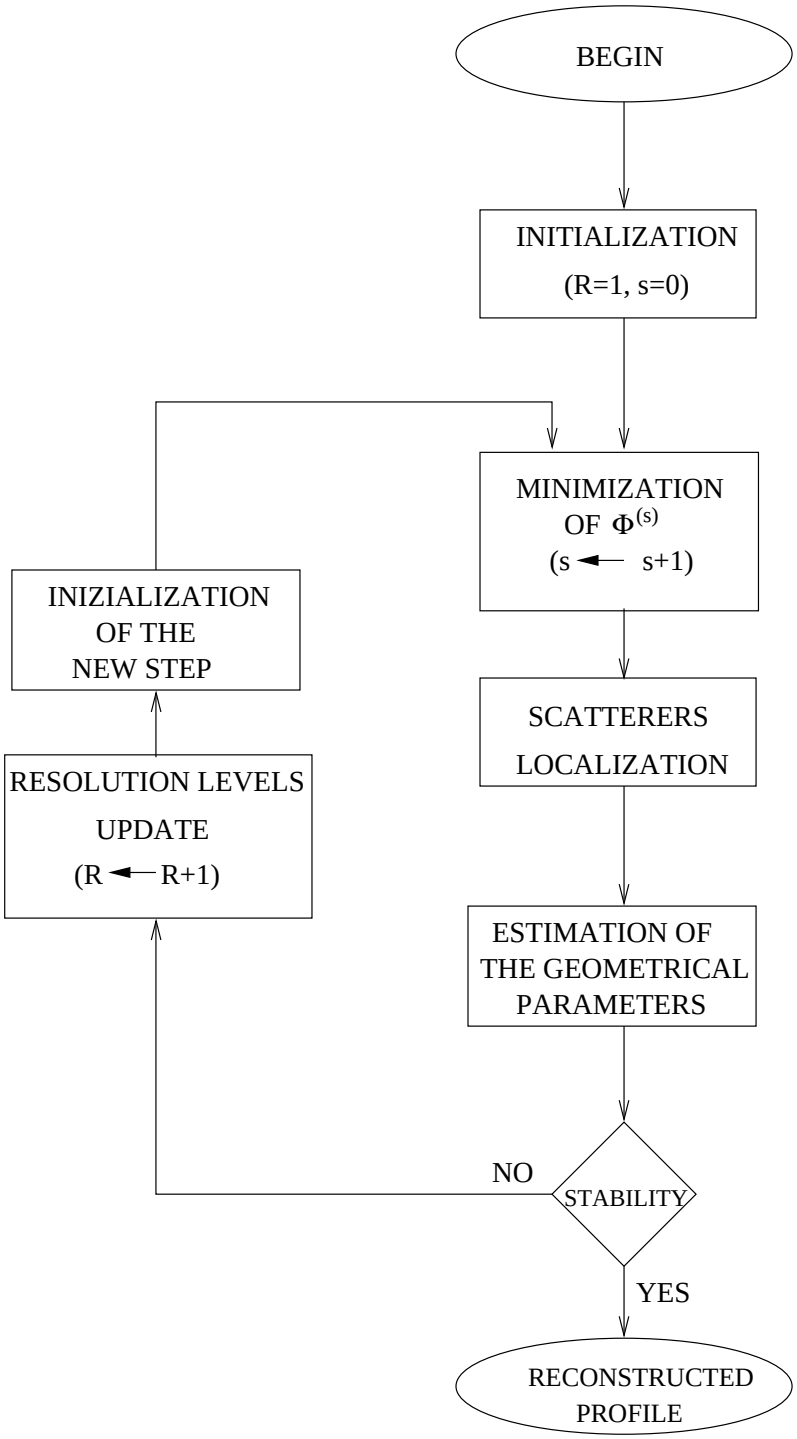


**Figure 2 - M. Donelli *et al.*,** "Effective Exploitation of Multi-View Data..."

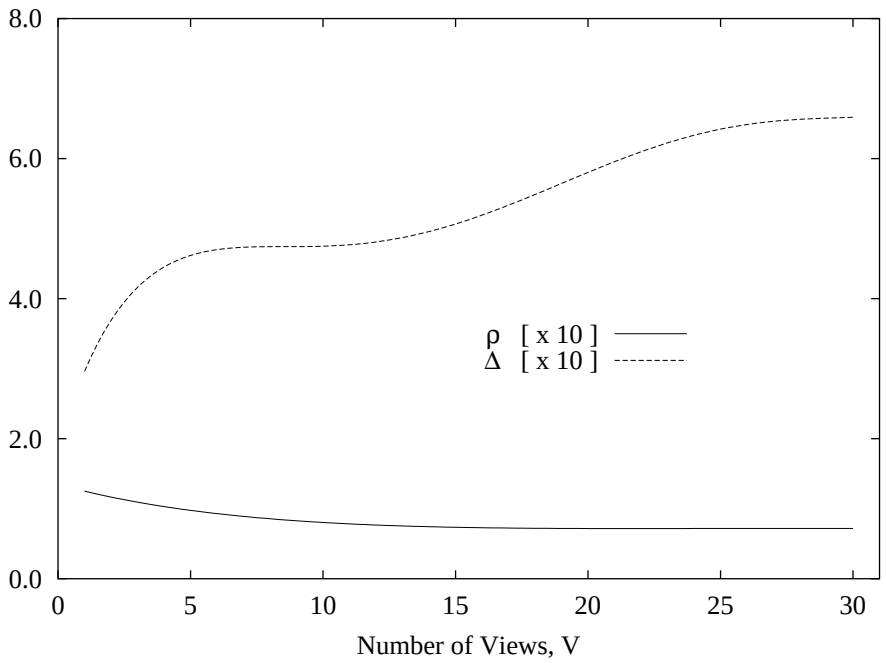


**Figure 3 - M. Donelli *et al.*,** "Effective Exploitation of Multi-View Data..."

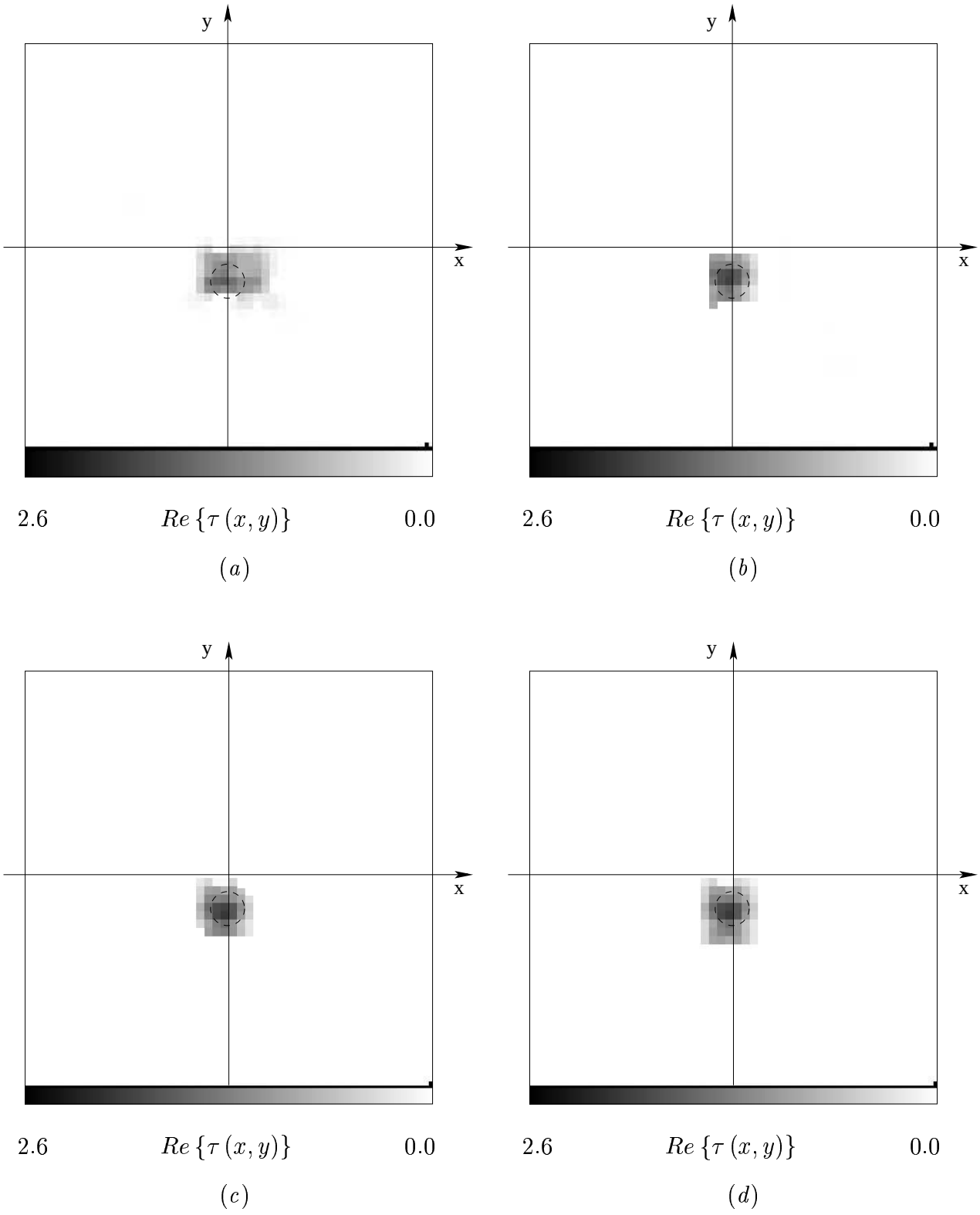


**Figure 4 - M. Donelli *et al.*,** "Effective Exploitation of Multi-View Data..."

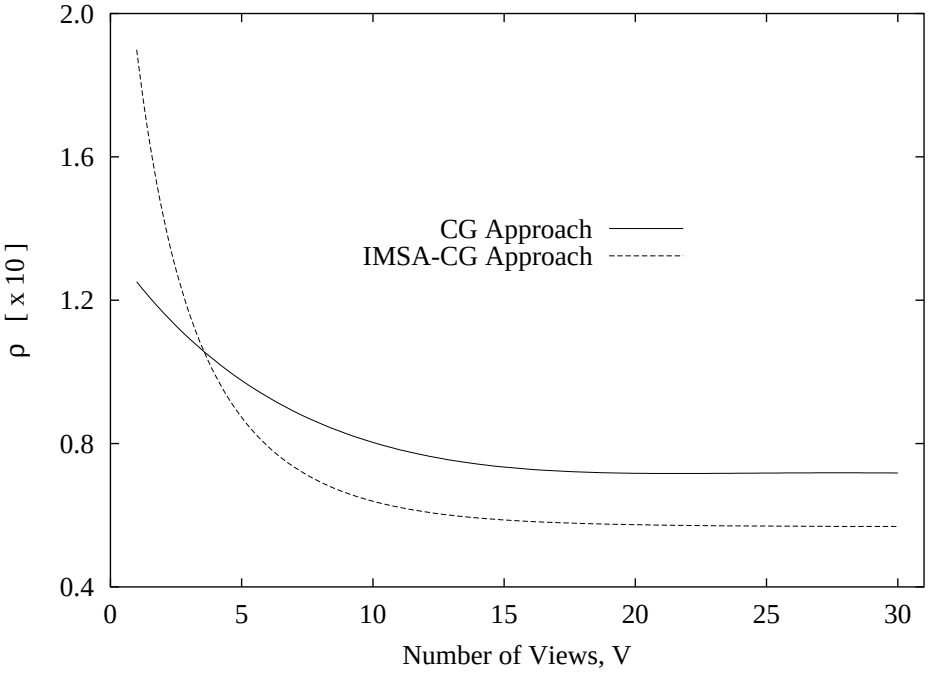


$(a)$

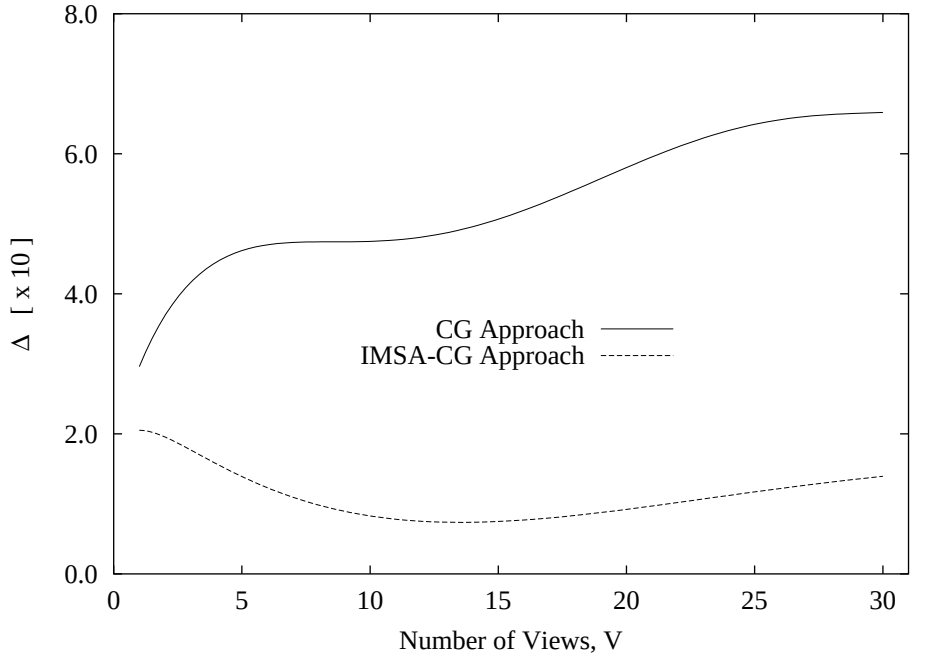


$(b)$

**Figure 5 - M. Donelli *et al.*,** "Effective Exploitation of Multi-View Data..."

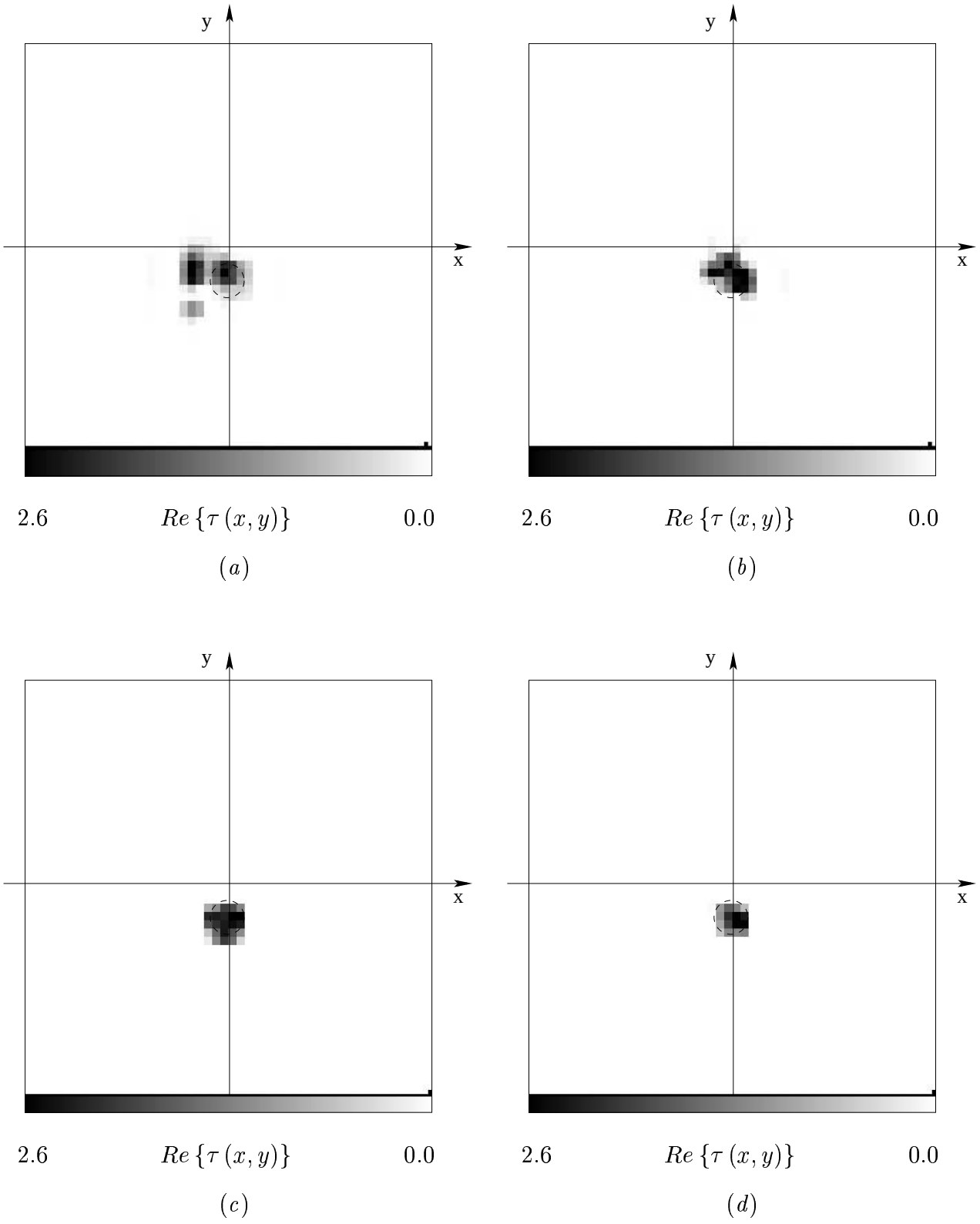


**Figure 6 - M. Donelli *et al.*,** "Effective Exploitation of Multi-View Data..."

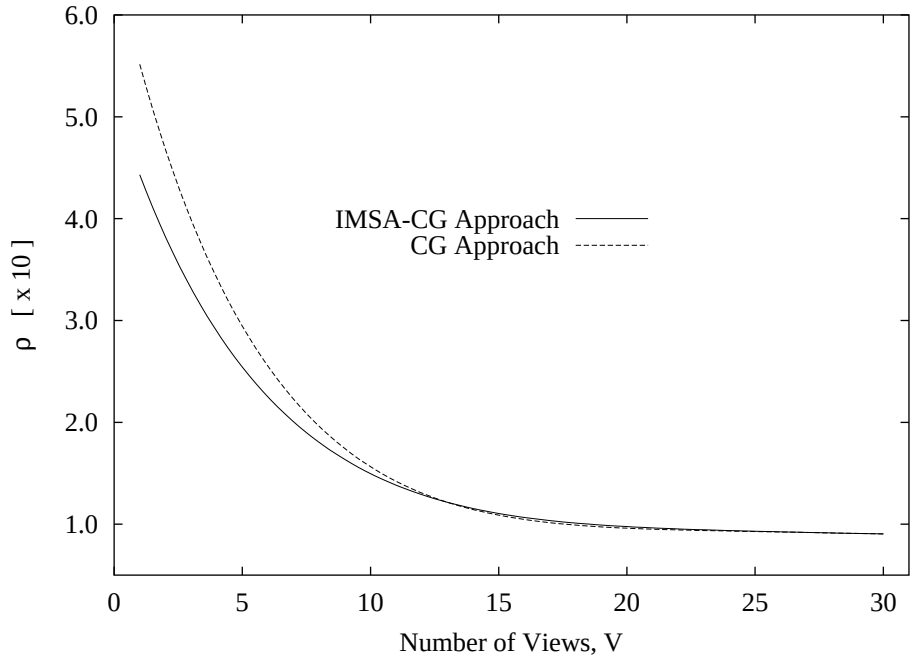


$(a)$

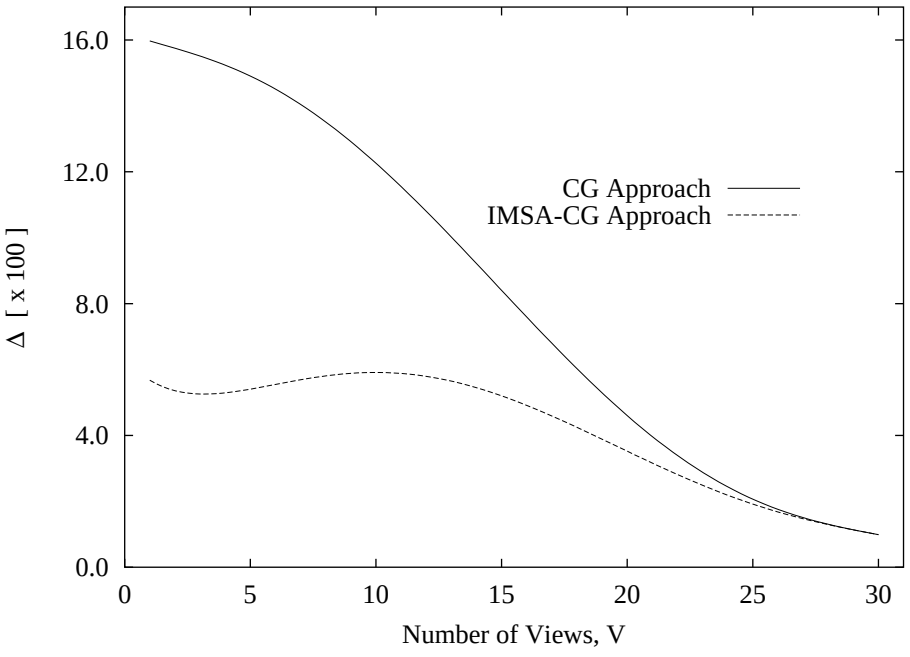


$(b)$

**Figure 7 - M. Donelli *et al.*,** "Effective Exploitation of Multi-View Data..."

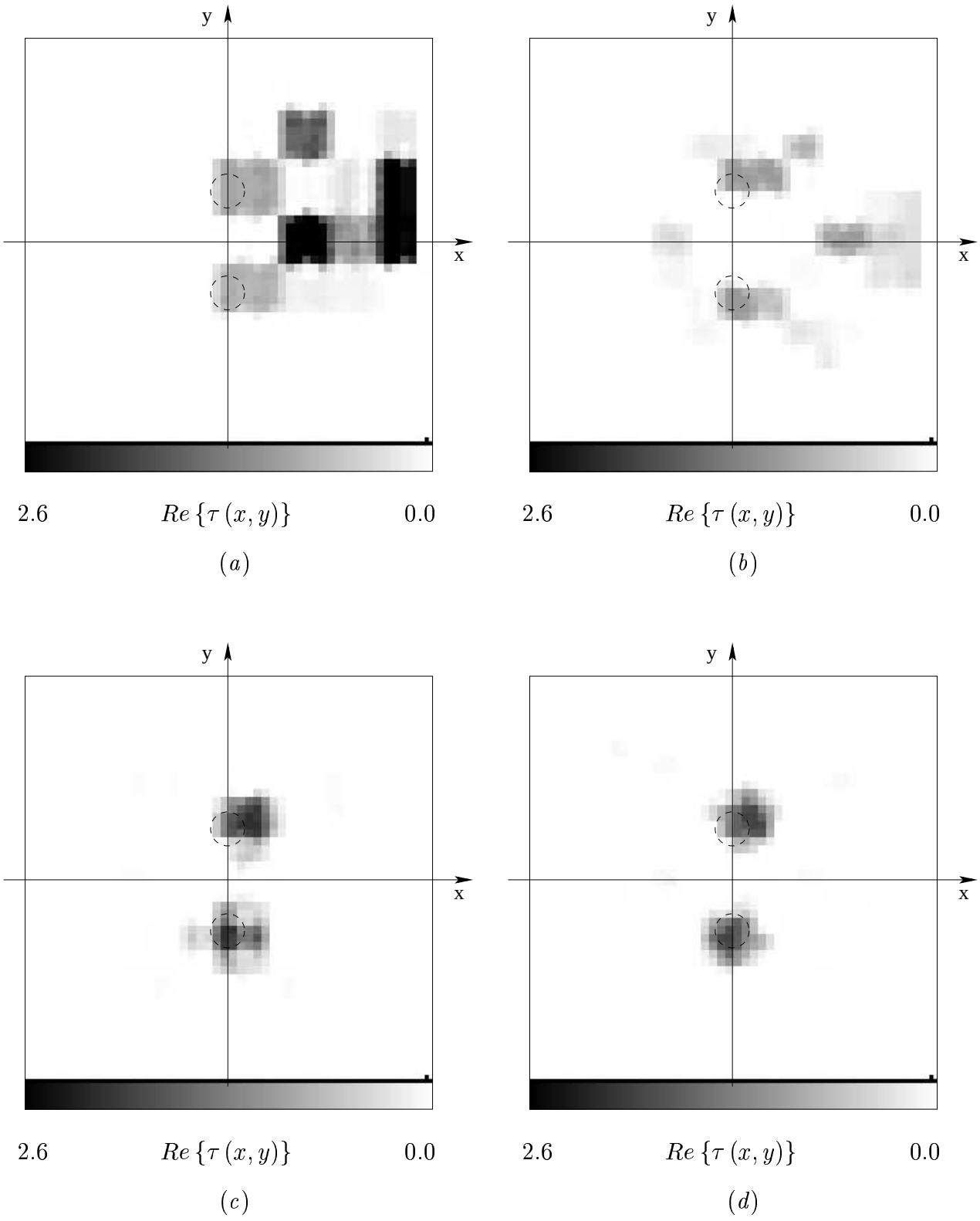


**Figure 8($I$) - M. Donelli *et al.*,** "Effective Exploitation of Multi-View Data..."

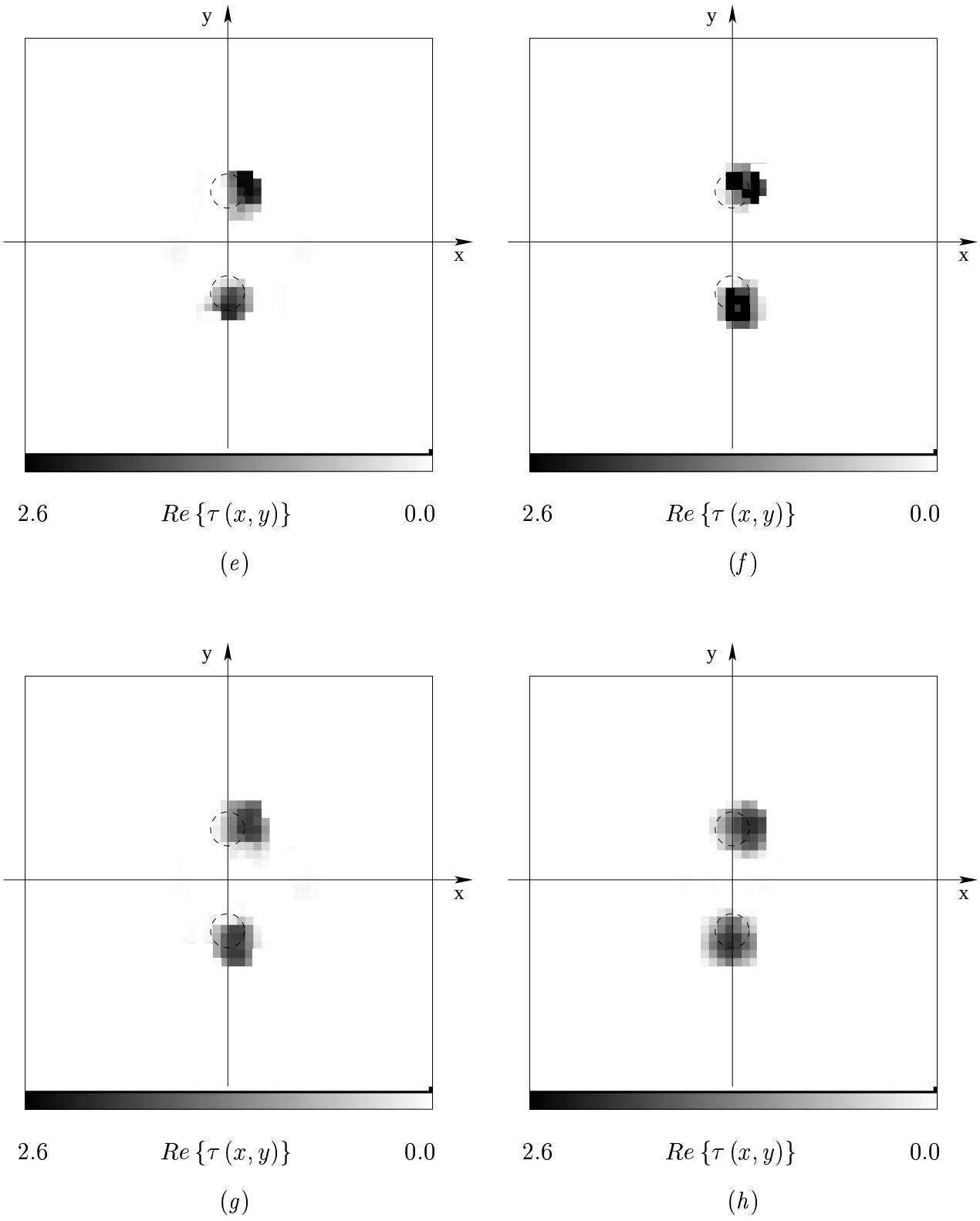


**Figure 8(*II*) - M. Donelli *et al.*,** "Effective Exploitation of Multi-View Data..."